Applied Catalysis B: Environmental 89 (2009) 255–264

Contents lists available at ScienceDirect

Applied Catalysis B: Environmental

journal homepage: www.elsevier.com/locate/apcatb

Solar photocatalytic degradation of persistent pharmaceuticals at pilot-scale: Kinetics and characterization of major intermediate products

Jelena Radjenović [a], Carla Sirtori [b], Mira Petrović [a,c], Damià Barceló [a,d], Sixto Malato [b,*]

[a] Department of Environmental Chemistry, IDAEA-CSIC, c/Jordi Girona 18-26, 08034 Barcelona, Spain
[b] Plataforma Solar de Almería (CIEMAT), Carretera Senes, Km. 4, 04200 Tabernas (Almería), Spain
[c] Institucio Catalana de Reserca i Estudis Avanzats (ICREA), Barcelona, Spain
[d] Institut Català de Recerca de l'Aigua (ICRA), Parc Científic i Tecnológic de la Universitat de, Girona, Pic de Peguera, 15, 17003 Girona, Spain

ARTICLE INFO

Article history:
Received 17 December 2008
Received in revised form 6 February 2009
Accepted 13 February 2009
Available online 27 February 2009

Keywords:
Acetaminophen
Atenolol
Intermediate products
Solar TiO_2 photocatalysis
Solar photo-Fenton
UPLC-QqToF–MS

ABSTRACT

The technical feasibility and performance of photocatalytic degradation of anti-inflammatory drug acetaminophen (ACTP) and β-blocker atenolol (ATL) have been studied in a well-defined system of a pilot-plant scale Compound Parabolic Collectors (CPCs) under natural illumination. Heterogeneous photocatalysis with titanium dioxide (TiO_2) and homogeneous photocatalysis by photo-Fenton were investigated with two different matrices: distilled water and synthetic municipal wastewater treatment plant effluent (S.E.). The initial concentrations of the pharmaceuticals studied were 10 mg L^{-1}, whereas the concentrations of the catalysts employed were 200 mg L^{-1} of TiO_2 and 5 mg L^{-1} of iron. Total disappearance of the parent compounds and discreet mineralization were attained in all experiments. Furthermore, kinetic parameters, release of heteroatoms and formation of carboxylic acids are discussed. The main intermediate products of photocatalytic degradation of atelonol has been structurally elucidated by tandem mass spectrometry (MS^2) experiments performed at quadrupole-time of flight (QqToF) mass analyzer coupled to ultra-performance liquid chromatograph (UPLC). Six transformation products were characterized, formed by consecutive attacks of hydroxyl ($^{\bullet}OH$) radical in concomitance with the disappearance of the primary compound. The proposed TiO_2 and photo-Fenton degradation route of ATL is reported for the first time.

1. Introduction

The presence of pharmaceuticals in the environment is an issue receiving growing attention worldwide. Possible adverse effects that pharmaceuticals might have in the ecosystems are still unknown, whereas many studies have been conducted on their occurrence in the aquatic and terrestrial environmental compartments [1–3].

Acetaminophen (ACTP) is a commonly used analgesic. After being processed in liver ACTP is excreted in urine [4]. Atenolol (ATL) is a β1 receptor specific antagonist, used primarily to treat cardiovascular diseases. After human consumption, it is excreted also via urine [5], with a small percentage of ATL-glucuronide (0.8–4.4%) and hydroxyATL (1.1–4.4%, hydroxylation of the benzilic position) [6]. The reported removals in sewage treatment plants (STPs) are varying from almost complete for ACTP [7], to no removal or partial removal reported for ATL [7,8]. As far as their photolysis in natural waters is concerned, Liu et al. [9] observed slow direct photolysis of ATL in water. Andrisano et al. [10] noticed an increase in the photodegradation rate of ATL with the decrease in pH in a UV-irradiated solution. The photodegradation rate of ACTP was found to follow the pseudo-first order kinetic in nitrate solution [11].

In recent years, advanced oxidation processes (AOPs) such as heterogeneous photocatalysis and photo-Fenton treatment have been gaining attention, especially in the treatment of water containing pharmaceuticals [12–15]. Heterogeneous photocatalysis is based on the use of wide band-gap semiconductors. When a semiconductor is illuminated with light energy greater than its band gap energy (BGE), excited high-energy states of electron and hole pairs (e−/h+) are produced. The photogenerated electrons could reduce the organic substrate [16] and the photogenerated holes can also oxidize either the organic molecule directly, or the OH^- ions and the H_2O molecules adsorbed on the catalyst's surface, to $^{\bullet}OH$ radicals. The most commonly used catalyst is titanium dioxide (TiO_2, BGE = 3.2 eV), because of its high reactivity, non-toxicity, low price and chemical stability [17,18]. One of the important advantages of heterogeneous photocatalysis is that solar spectrum can be used to photoexcite the semiconductor catalyst, thus surpassing the cost of UV radiation. In the photo-Fenton method, the reagents used for the

* Corresponding author. Tel.: +34 950387940; fax: +34 950365015.
E-mail address: Sixto.Malato@psa.es (S. Malato).

0926-3373/$ – see front matter © 2009 Elsevier B.V. All rights reserved.
doi:10.1016/j.apcatb.2009.02.013

oxidation of organic compounds are Fe^{2+} salts and hydrogen peroxide (H_2O_2), which is non-toxic and environmentally safe mixture. The UV–vis light enhances the reaction through accelerating the regeneration of the ferrous ions and increasing the formation of •OH radicals [19].

However, radical-induced reactions occurring in photocatalytic treatments will evolve through complex parallel consecutive pathways of intermediate products. Since hydroxyl-radicals are not selective, various by-products are formed at low concentration levels. The identification of these intermediates and determination of kinetics of their degradation is crucial due to their potential presence in the effluent of the treatment, and apprehension of their degradation pathways in order to determine the key steps of photodecomposition. Moreover, elucidation of mechanisms of photocatalytic reactions can help in gaining information on naturally occurring transformations, such as the case of intermediate photocatalytic products of atrazine that were encountered in soil samples [20], and metabolic products of a doping substance buspirone extracted from the animal liver [21].

The knowledge on photocatalytic intermediates of pharmaceuticals is still scarce [22–26]. Lambropoulou et al. [24] identified 17 products of photocatalytic degradation of bezafibrate. Pérez-Estrada et al. [23] elucidated the photo-Fenton degradation pathway of diclofenac. Zhang et al. [26] proposed a pathway for photocatalytic degradation of acetaminophen via direct hole oxidation and *ipso*-substitution. Zbaida et al. [25] identified several intermediate products of reaction of cimetidine with Fenton reagent (Fe^{2+}/H_2O_2), such as cimetidine sulfoxide, N-desmethylcimetidine, N-desmethylcimetidine sulfoxide, cimetidine guanylurea and 5-hydroxymethylimidazole derivative of cimetidine sulfoxide. As far as ATL is concerned, Liu et al. [9] observed its slow direct photolysis, whereas for propranolol three photodegradation products of aromatic ring oxidation and opening were identified. In the experiments with 5 mL TiO_2 suspensions under simulated solar light, Medana et al. [27] identified several transformation products of ATL, mainly mono-, di- and tri-hydroxilated derivatives.

This study describes the oxidation of ACTP and ATL at pilot-scale Compound Parabolic Collector (CPC) under natural illumination. Two widely used AOP systems, TiO_2 and photo-Fenton solar photocatalysis, were investigated with two types of matrix: distilled water and SE. The specific aim of this study was to investigate the kinetics of the processes and determine the influence that the matrix might have when applying the two abovementioned AOPs for the treatment of wastewater. Since these pharmaceuticals are frequently detected in STP effluents, it is important to evaluate the possible influence of this matrix on the process efficiency. Special attention has been paid to identify the main intermediate products of ATL formed during the treatment. ACTP was not included in the study as its structure is so similar to ATL (and simpler) and due to a previous study already published by Medana et al. [27]. The major transformation products of photo-Fenton and TiO_2 photocatalysis of ATL have been characterized by accurate mass measurements of the tandem mass spectrometry (MS^2) spectra obtained at quadrupole-time of flight (QqToF) instrument, coupled to ultra-performance liquid chromatography (UPLC) system. Possible photocatalytic degradation pathways of the two therapeutic drugs were proposed, whereas the reactions involved either oxidation by the •OH radical or reduction by conduction band electrons.

2. Experimental

2.1. Chemicals

The test substances and analytical standards for chromatography analysis for ACTP ($C_8H_9NO_2$) and ATL ($C_{14}H_{22}N_2O_3$) were purchased from Sigma–Aldrich (Scheme 1). Distilled water used in both pilot plants was obtained from the Plataforma Solar de Almería (PSA) distillation plant (conductivity < 10 μS cm^{-1}, Cl^- = 0.7–0.8 mg L^{-1}, NO_3^- = 0.5 mg L^{-1}, organic carbon < 0.5 mg L^{-1}). The heterogeneous photocatalytic degradation tests were carried out using a slurry suspension (200 mg L^{-1} TiO_2) of Degussa (Frankfurt, Germany) P-25 TiO_2 (surface area 51–55 m^2 g^{-1}, size of the primary particles: 30–50 nm, 80% anatase, 20% rutile). Photo-Fenton experiments were performed using iron sulfate ($FeSO_4{\cdot}7H_2O$), reagent-grade hydrogen peroxide (30% w/v) and sulfuric acid for pH adjustment. The chemical composition of the synthetic municipal wastewater treatment plant effluent (S.E.) was adapted of OECD Guidelines for Testing of Chemicals [28]: Peptone (32 mg L^{-1}), meat extract (22 mg L^{-1}), urea (6 mg L^{-1}), K_2HPO_4 (28 mg L^{-1}), $CaCl_2.2H_2O$ (4 mg L^{-1}), NaCl (7 mg L^{-1}) and $Mg_2SO_4.7H_2O$ (2 mg L^{-1}), TOC = 20 mg L^{-1}.

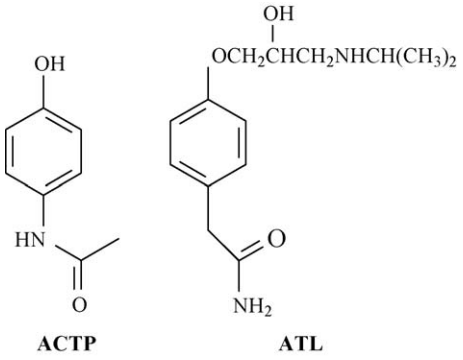

Scheme 1. Chemical structures of ACTP and ATL.

2.2. Experiment set-up

All experiments were carried out under sunlight in a pilot plant at the PSA (latitude 37°N, longitude 2.4°W). A compound parabolic collector field (CPC) has been used for the photocatalytic degradation assays. The pilot plant operates in batch mode and it has been described in detail in previous works [29]. It basically consists of 2 modules connected in series containing each 8 parallel reflectors (3.2 m^2, polished aluminium) with UV transparent tubular receivers (i.d. 48 mm). The contaminated water flows directly from one to the other and finally to a reservoir tank. A centrifugal pump then returns the water to the collectors in a closed circuit. The overall capacity of the reactor (V_T) is 150 L. It is consists of 36 L of total irradiated volume (V_i) and the dead reactor volume (tank + high density polyethylene tubes. 114 L). The experiments were performed during May 2008, between 9 a.m. and 4 p.m.

Solar UV radiation was measured by a global UV radiometer (KIPP&ZONEN, model CUV 4), mounted on a platform tilted 37° (the same as the CPCs), which provides data in terms of incident W_{UV} m^{-2}. In this way, the energy reaching any surface in the same position with regard to the sun is measured. With Eq. (1), combination of the data from several days' experiments and their comparison with other photocatalytic experiments is possible.

$$t_{30\,W,n} = t_{30\,W,n-1} + \Delta t_n \frac{UV}{30}\frac{V_i}{V_T}; \quad \Delta t_n = t_n - t_{n-1} \tag{1}$$

where t_n is the experimental time for each sample, UV is the average solar ultraviolet radiation measured during Δt_n, and t_{30W} is a "normalized illumination time". In this case, time refers to a constant solar UV power of 30 W m^{-2} (typical solar UV power on a perfectly sunny day around noon).

At the beginning of all the photo-Fenton experiments, a concentrated solution of the compound was directly added to the photoreactor, and a sample was taken after 15 min of homogenisation (initial concentration). Then the pH was adjusted with sulfuric acid and another sample was taken after 15 min to confirm the pH. Afterwards, iron salt was also added ($FeSO_4{\cdot}7H_2O$) and homogenized well for 15 min before the next sample was taken. Finally an initial dose of H_2O_2 was added, the collector was uncovered and samples were taken to evaluate the degradation process. Photo-Fenton experiments were carried out at a pH adjusted to 2.6–2.8 as proposed and Fe^{2+} concentration of 5 mg L^{-1}. In the kinetic study, the initial hydrogen peroxide concentration was around 10 mg L^{-1} and was maintained in excess during the experiments.

For TiO_2 photocatalysis experiments, first the compound was added to the pilot plant, and homogenized for 15 min, and then a sample of the initial concentration was taken. Finally, the catalyst TiO_2 (200 mg L^{-1}) was added. After 15 min, another sample was taken for evaluating parent compound adsorption on catalyst and the collector was uncovered.

The initial concentration of the investigated pharmaceuticals was 10 mg L^{-1}. Although this value is significantly higher than the environmental concentration of ACTP and ATL it was chosen for better evaluating the kinetics. Moreover, at lower concentrations of organic compound the photodegradation can be expected to be quicker, for the same concentrations of iron and H_2O_2. Therefore, the obtained results could be considered really conservative concerning treatment times.

2.3. Analytical determinations

Mineralization was followed by measuring the Dissolved Organic Carbon (DOC) by direct injection of filtered samples into a Shimadzu-5050A TOC analyser provided with an NDIR detector and calibrated with standard solutions of potassium phthalate.

The concentrations of pharmaceuticals were analyzed using reverse-phase liquid chromatography (flow rate 0.5 mL min^{-1}) with UV detector in an HPLC-UV (Agilent Technologies, series 1100) with C-18 column (LUNA 5 μm, 3 mm × 150 mm from Phenomenex). Ultra pure distilled–deionized water obtained from a Milli-Q (Millipore Co.) system and HPLC-graded organic solvents were used to prepare all the solutions. The mobile phase composition and wavelength in each case was: for ACTP formic acid (25 mM)/acetonitrile (92/8) at 250 nm; for ATL formic acid (25 mM)/acetonitrile (95/5) at 228 nm.

Ammonium concentration was determined with a Dionex DX-120 ion chromatograph (IC) equipped with a Dionex Ionpac CS12A 4 mm × 250 mm column. Isocratic elution was done with H_2SO_4 (10 mM) at a flow rate of 1.2 mL min^{-1}. Anion concentrations (NO_3^-) were measured with a Dionex DX-600 ion chromatograph using a Dionex Ionpac AS11-HC 4 mm × 250 mm column. The gradient program was pre-run for 5 min with 20 mM NaOH, an 8-min injection of 20 mM of NaOH, and 7-min with 35 mM of NaOH, at a flow rate of 1.5 mL min^{-1}.

Total iron concentration was monitored by colorimetric determination with 1,10-phenanthroline, according to ISO 6332, using a Unicam-2 spectrophotometer. The concentration of H_2O_2 was analyzed by a fast, simple spectrophotometric method using ammonium metavanadate, which allows the H_2O_2 concentration to be determined immediately based on a red-orange peroxovanadium cation formed during the reaction of H_2O_2 with metavanadate, maximum absorption of which is at 450 nm. The H_2O_2 concentrations are calculated from absorption measurements by a ratio found by Nogueira et al. [30].

2.4. UPLC/ESI-QqToF–MS analysis

The identification of photodegradation products was carried out on the samples concentrated 50-fold by solid-phase extraction (SPE), and samples without the preconcentration step. For the SPE a Baker vacuum system (J.T. Baker, The Netherlands) and Oasis HLB cartridges (60 mg, 3 mL) from Waters Corporation (Milford, MA) were used, previously conditioned at neutral pH with 5 mL of methanol followed by 5 mL of deionised water (HPLC grade). Accurate mass spectrometry (MS) and MS^2 analyses of ATL and its photocatalytic transformation products were performed using a Waters/Micromass QqToF-MicroTM system coupled to Waters ACQUITY UPLCTM system (Micromass, Manchester, UK). Samples were analyzed on a Waters ACQUITY BEH C18 column (10 mm × 2.1 mm, 1.7 μm particle size). After elution from the column, the compounds were analyzed in positive ion (PI) mode with a mobile phase consisting of (A) 5 mM aqueous NH_4Ac/acetic acid (pH 4.8) and (B) acetonitrile–methanol (2:1, v/v) at 400 μL min^{-1}. The elution started at 5% B for 1 min and then it was linearly increased to 60% of B in 8 min, further increased to 95% of B in the next 2 min, and then returned to initial conditions. Total run time, including the conditioning of the column to the initial conditions was 14 min. The injection volume of the sample was 10 μL.

The mass spectrometry analysis on the QqToF instrument was performed in wide pass quadrupole mode, for MS experiments, with the ToF data being collected between m/z 50 and 700. The capillary and cone voltages were set to 3000 and 25 V, respectively. Data were collected in the centroid mode, with a scan accumulation time of 1 s. The instrument was operated at a resolution of 5000 (FWHM). The nebulisation gas was set to 500 L/h at a temperature of 350 °C, the cone gas was set to 50 L/h, and the source temperature to 120 °C. All analyses were acquired using an independent reference spray via the LockSpray interference to ensure accuracy and reproducibility. Sulfaguanidine was used as the internal lock mass in the PI mode with $[M+H]^+ = m/z$ 215.0602. The LockSpray frequency was set at 11 s. Fragmentation of precursor ions was done by applying collision energies in the range of 10–50 eV, using argon as a collision gas at a pressure of ~20 psi.

Elemental compositions of the molecular ions and their fragments were determined and exact masses were calculated with the help of MassLynx V4.1 software incorporated in the instrument. Since the software calculation of the accurate mass of cation is performed by adding a hydrogen atom instead of proton, mass of one electron (i.e., 0.0005) was subtracted from the calculated mass [31].

3. Results and discussion

3.1. Hydrolysis and photolysis

Previous to the photocatalytic treatments photolysis and hydrolysis experiments were performed to know the contribution of these effects. Photolysis was performed for each compound at natural pH in water in 5-l Pyrex beakers (UV transmissivity >80% between 320 and 400 nm, around 40% at 300 nm, 15 cm internal diameter). Beakers were exposed to direct sunlight and continuously stirred during the photolysis tests. The maximum temperature inside the beakers was 35 °C. Hydrolysis experiments were performed using 250-mL amber glass bottles, which were kept in the dark during the tests. Photolysis and hydrolysis experiments started with a concentration around 10 mg L^{-1} of each compound. The experiments showed no phototransformation of the investigated compounds in the dark or under solar irradiation, whereas the concentration of primary drugs and

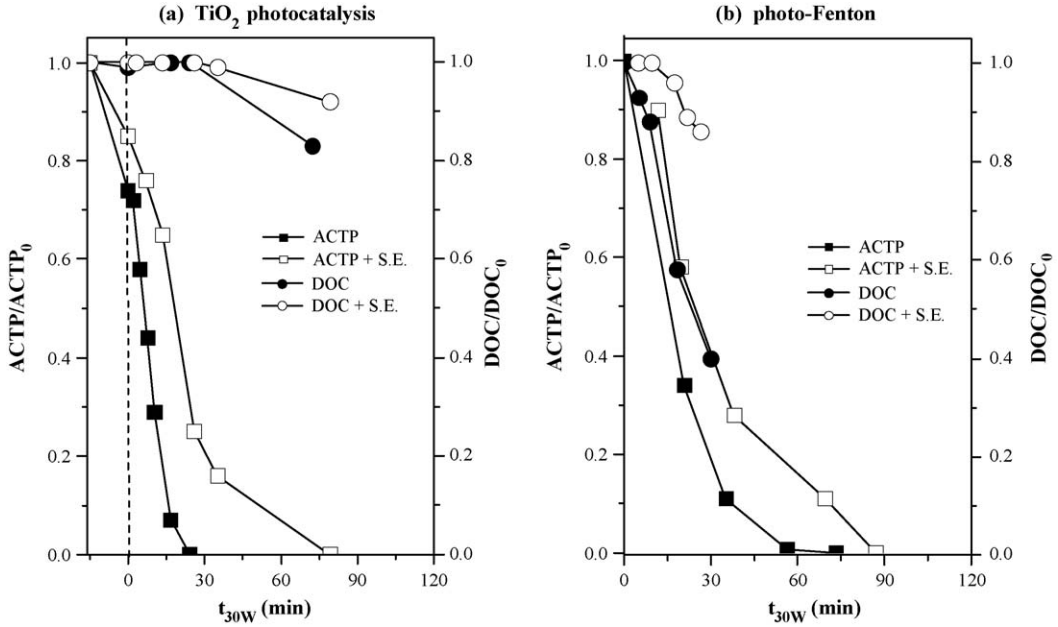

Fig. 1. Degradation and mineralization of ACTP by: (a) TiO_2 photocatalysis, and (b) photo-Fenton experiments.

DOC were constant after 10 h, much longer time than used during the photocatalytic tests.

3.2. Photocatalytic degradation of ACTP

25% of the initial ACTP concentration was adsorbed onto the catalyst in the dark, prior to illumination. In distilled water by TiO_2, the concentration of ACTP decreased rapidly, during the first 6 min of irradiation 50% of ACTP was degraded, and completely disappeared after 24 min of illumination time (see Fig. 1a). DOC was stable, showing a substantially slower mineralization at around 21% at the end of the treatment (72.2 min of irradiation). This can be explained by the formation of oxidation intermediates of ACTP, which were also observed at the HPLC diode array detector scans as signals at 250 nm wavelength. However, ACTP was degraded notoriously more slowly during the TiO_2 photocatalysis with the S.E. than in distilled water. In this case, the compound was totally degraded at around 79.1 min of illumination time. A very discreet mineralization (11%) was observed at the end of the process. Therefore, it can be concluded that other organics present in the S.E. could compete for the hydroxyl radicals and provoked a lower ACTP degradation rate and a not significant mineralisation.

The photo-Fenton experiments were performed using a 5 mg L^{-1} iron concentration and H_2O_2 was maintained between 10 and 20 mg L^{-1}. In the experiments with distilled water, all the initial concentration of ACTP was degraded at 12 min of illumination time (see Fig. 1b). At this point DOC had decreased by around 22%. For SE, photo-Fenton showed slow degradation and mineralization. ACTP was totally removed at around 21.8 min. of illumination time. At this point, a discreet decrease in DOC (11%) was observed, and then up to 34.2 min, remained at a plateau at around 25 mg L^{-1}. Concerning hydrogen peroxide consumption in S.E., two stages could be observed during ACTP treatment. The first one, with a substantial H_2O_2 consumption when ACTP was present in the solution (2.5 mM of H_2O_2 were necessary for degrading completely ACTP), and the second stage after total elimination of ACTP, when the H_2O_2 was consumed slower. The negative influence of STP effluent matrix has been confirmed recently for photo-Fenton degradation of other pharmaceuticals [32]. This was explained by the presence of organic compounds that present absorbance in the same region as the ferric iron complexes, and thus can reduce its radiation absorption, hindering the regeneration of Fe(II).

3.3. Photocatalytic degradation of ATL

During TiO_2 photocatalysis, no significant adsorption of ATL onto TiO_2 photocatalyst was observed, both in distilled and synthetic wastewater (see Fig. 2a). Additionally, degradation of ATL in the experiments with distilled water was faster than in S.E. with 50% of its initial concentration decreased during the first 4.8 min of irradiation, whereas the compound completely disappeared after 33.4 min. On the other side, DOC determinations showed a not substantial mineralization (around 40%) after 120 min. For S.E. matrix, 90% of ATL was degraded at around 72 min of illumination time. At this point, only 13% of the initial organic carbon had been mineralized, which indicates the formation of abundant intermediate products of oxidation, not only from ATL but from other compounds formed from the organic content of S.E.

The photo-Fenton experiment in distilled water presented a complete and very fast disappearance of ATL (<3.8 min of illumination time, corresponding to first sampling after illumination). For this reason, the data related with its degradation was not illustrated at the corresponding figure (see Fig. 2b). In its turn, DOC had decreased 74% after 35.5 min of irradiation. On the other hand, for SE, ATL completely disappeared after at around 30 min of treatment. The decrease in DOC was very slowly and, only 13% of the initial organic matter was mineralized when ATL was completely eliminated. Concerning hydrogen peroxide consumption in S.E., 2.9 mM of H_2O_2 were necessary for degrading completely ATL.

3.4. Kinetics

The kinetic studies were also performed for each compound, assuming that the reaction between the $^{\bullet}OH$ radicals and the pharmaceutical is the rate-determining step as initial concentration was rather low (10 mg L^{-1}). Degradation in all the experiments may be described by a pseudo-first order reaction rate (r),

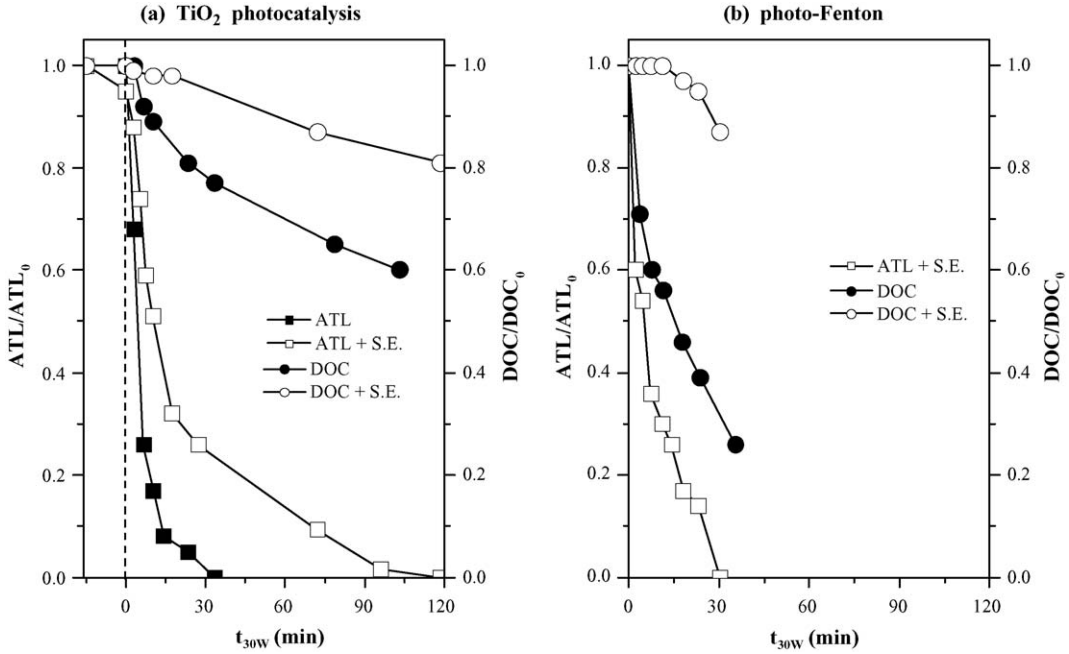

Fig. 2. Degradation and mineralization of ATL by: (a) TiO_2 photocatalysis, and (b) photo-Fenton experiments.

where C represents the concentration of ACTP and ATL, k_{OH} is the reaction rate constant and k_{ap} is a pseudo-first order constant taking into account that $^{\bullet}OH$ radicals concentration could be considered constant (see Eq. (2)). It is necessary to remark that $^{\bullet}OH$ radicals concentration depends on catalyst concentration (TiO_2 or Fe) and photons absorbed by each catalytic system.

$$r = k_{OH}[^{\bullet}OH]C = k_{ap}C \quad (2)$$

This was confirmed by the linear behavior of $\ln(C_0/C)$ as a function of t_{30w}, in all the experiments performed. In Table 1 are summarized the kinetic constants and the half-life times ($t_{1/2}$) calculated for each compound in both matrices, when treated with photo-Fenton or TiO_2. From the data presented, it can be concluded that photo-Fenton is more effective than TiO_2 for ACTP and ATL.

Nitrogen inorganic species (NH_4^+ and NO_3^-) were monitored for the three compounds studied in distilled water matrix. The concentrations encountered were very low (0.2 mg NH_4^+ L^{-1} for ACTP and 0.56 mg NH_4^+ L^{-1} for ATL; 0.1 mg NO_3^- L^{-1} for ACTP and for ATL the analysis showed a concentration below than 0.1 mg NO_3^- L^{-1}). Indeed the N contents of 10 mg L^{-1} of ACTP and ATL are 0.9 mg $L^{-1}$and 1.1 mg L^{-1}, respectively. Therefore, the expected concentration of NH_4^+ or NO_3^-, supposing that all nitrogen could be mineralised, is quite low. ACTP was mineralized into NH_4^+ (0.35 mg L^{-1}) and mostly nitrate ions (0.18 mg NO_3^- L^{-1}), whereas for ATL only NH_4^+ ions were detected (0.37 mg NH_4^+ L^{-1}). This result indicated that the $^{\bullet}OH$ radical attack probably occurred on the nitrogen instead on the carbon atom, which lead to NH_4^+ formation [33].

The evolution of six carboxylic acids (i.e., acetic, oxalic, maleic, propionic, pyruvic and formic acid) in the photocatalytic experiments with distilled water was also monitored. Carboxylic and dicarboxylic acids are known to form stable iron complexes, which inhibit the reaction with H_2O_2, thus they are usually degraded slowly compared with other organics in the photo-Fenton process [34]. In general, organic acids are the last step before complete mineralisation. The analyses allowed determining maleic and formic acid as the final products of the TiO_2 photocatalysis of ACTP (see Fig. 3a). The final concentration of maleic acid was determined to be around 9 mg L^{-1}, whereas the concentration of formic acid was 1.2 mg L^{-1} at the same point. In this case, 56% of remaining DOC could be attributed to the carboxylic acids mentioned previously. At the end of the photo-Fenton process, formic and acetic acid were present at lower concentrations (see Fig. 3b). According to Pérez-Estrada et al. [35] the poorer concentration of carboxylic acids in the end of the processes and, especially during

Table 1
Kinetic parameters determined for the TiO_2 photocatalysis and photo-Fenton reactions of the compounds studied.

Compound	Matrix	TiO_2 photocatalysis		photo-Fenton	
		k_{ap} (min^{-1})	r^2	k_{ap} (min^{-1})	r^2
ACTP	Distilled	0.1062	0.9905	0.2477	0.9931
	S.E.	0.0594	0.9894	0.1314	0.9968
ATL	Distilled	0.1810	0.9871	[a]	[a]
	S.E.	0.0689	0.9950	0.0827	0.9686

[a] Insufficient data for calculate the kinetic parameters (rapid ATL degradation).

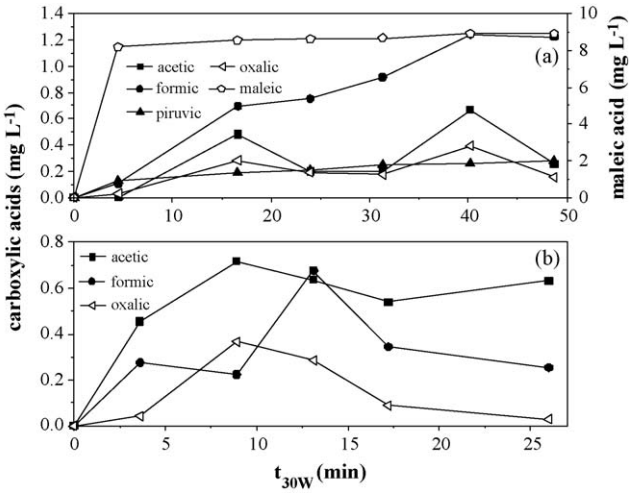

Fig. 3. Carboxylic acids released during degradation of ACTP in the experiments with distilled water: (a) TiO_2 photocatalysis, and (b) photo-Fenton photocatalysis.

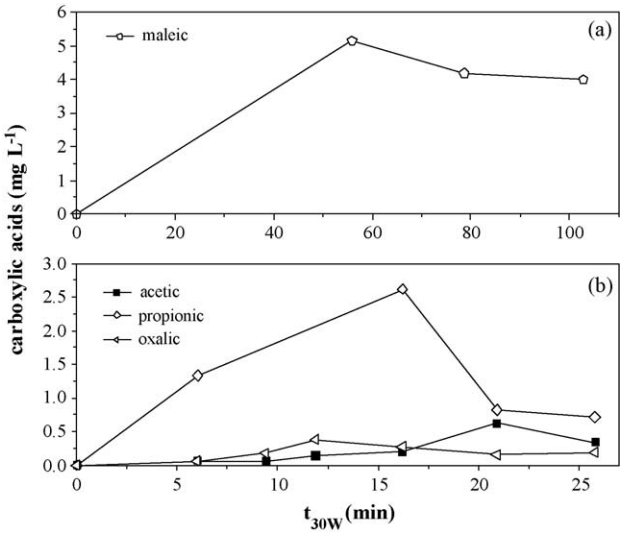

Fig. 4. Carboxylic acids released during degradation of ATL in the experiments with distilled water: (a) TiO_2 photocatalysis, and (b) photo-Fenton photocatalysis.

photo-Fenton, could be justified due to the continuous forming and degrading of carboxylic acids. For this reason, these end-products could not be accumulated and, consequently determined, at any significant concentration. This is concomitant with a fast degradation of DOC, as shown in Fig. 1. The results of IC analysis for experiments with ATL corroborate with the previous observations (see Fig. 4(a and b)). In the TiO_2 photocatalytic experiments with ATL only maleic acid was determined at a final concentration at around 4 mg L^{-1}, as treatment time was not long enough for permitting the formation of substantial quantities of smaller carboxylic acids. At the end of photo-Fenton treatment, oxalic, acetic and propionic acid were determined at concentrations below 0.5 mg L^{-1}, which is consistent with the rapid ATL degradation and substantial mineralisation at the end of the treatment.

3.5. Characterization of major intermediate of ATL degradation products by UPLC/ESI-QqToF

In order to detect possible intermediate products of the selected pharmaceuticals, samples with and without the preconcentration step from TiO_2 and photo-Fenton experiments, with both types of

Table 2
Accurate mass measurement of product ions of atenolol (ATL) and its photodegradation products as determined by UPLC/ESI-QqToF in MS/MS mode. Only product ions with abundances higher than 10% are taken into account.

Compound	Precursor ion/Product ion	Elemental formula	Mass (*m*/*z*)		Error		DBE[a]
			Experimental	Theoritical	mDa	ppm	
ATL	$[M+H]^+$	$C_{14}H_{23}N_2O_3$	267.1702	267.1704	−0.2	−0.7	4.5
	$[M+H\text{-}C(CH_3)_2]^+$	$C_{11}H_{17}N_2O_3$	225.1240	225.1234	0.6	2.7	4.5
	$[M+H\text{-}NH_2CH(CH_3)_2]^+$	$C_{11}H_{14}NO_3$	208.0974	208.0969	0.5	2.4	5.5
	$[M+H\text{-}NH_2CH(CH_3)_2\text{-}H_2O]^+$	$C_{11}H_{12}NO_2$	190.0869	190.0863	0.6	3.2	6.5
	$[M+H\text{-}NH_2CH(CH_3)_2\text{-}H_2O\text{-}CO\text{-}NH_3]^+$	$C_{10}H_9O$	145.0653	145.0648	0.5	3.4	6.5
	$[M+H\text{-}NH_2CH(CH_3)_2\text{-}H_2O\text{-}CHCONH_2]^+$	C_9H_9O	133.0660	133.0648	1.2	9.1	5.5
	$[M+H\text{-}HOC_6H_4CH_2CONH_2]^+$	$C_6H_{14}NO$	116.1065	116.1070	−0.5	−4.3	0.5
P237	$[M+H]^+$	$C_{13}H_{20}NO_3$	238.1444	238.1438	0.6	2.5	4.5
	$[M+H\text{-}H_2O]^+$	$C_{13}H_{18}NO_2$	220.1336	220.1332	0.4	1.8	5.5
	$[M+H\text{-}C(CH_3)_2]^+$	$C_{10}H_{14}NO_3$	196.0965	196.0968	−0.3	−1.5	4.5
	$[M+H\text{-}C(CH_3)_2\text{-}H_2O]^+$	$C_{10}H_{12}NO_2$	178.0861	178.0863	−0.2	−1.1	5.5
	$[M+H\text{-}NH_2CH(CH_3)_2\text{-}H_2O]^+$	$C_{10}H_9O_2$	161.0608	161.0597	1.1	6.8	6.5
	$[M+H\text{-}CH_2NHCH(CH_3)_2\text{-}OH]^+$	$C_9H_9O_2$	149.0607	149.0597	1.0	6.7	5.5
	$[M+H\text{-}H_2O\text{-}NHCH(CH_3)_2\text{-}CHO]^+$	C_9H_9O	133.0654	133.0648	0.6	4.5	5.5
	$[M+H\text{-}HOC_6H_4CHO]^+$	$C_6H_{14}NO$	116.1065	116.1070	−0.5	−4.3	0.5
P253	$[M+H]^+$	$C_{13}H_{20}NO_4$	254.1385	254.1387	−0.2	−0.8	4.5
	$[M+H\text{-}H_2O]^+$	$C_{13}H_{18}NO_3$	236.1287	236.1281	0.6	2.5	5.5
	$[M+H\text{-}C(CH_3)_2]^+$	$C_{10}H_{14}NO_4$	212.0920	212.0917	0.3	1.4	4.5
	$[M+H\text{-}C(CH_3)_2\text{-}H_2O]^+$	$C_{10}H_{12}NO_3$	194.0833	194.0812	2.1	10.8	5.5
	$[M+H\text{-}NH_2CH(CH_3)_2\text{-}H_2O]^+$	$C_{10}H_9O_3$	177.0547	177.0546	0.1	0.6	6.5
	$[M+H\text{-}\ NH_2CH(CH_3)_2\text{-}H_2O\text{-}C_2H_2]^+$	$C_8H_7O_3$	151.0396	151.0390	0.6	4.0	5.5
	$[M+H\text{-}H_2O\text{-}NHCH(CH_3)_2\text{-}O\text{-}CHO]^+$	C_9H_9O	133.0646	133.0648	−0.2	−1.5	5.5
	$[M+H\text{-}HOC_6H_3(OH)CHO]^+$	$C_6H_{14}NO$	116.1052	116.1070	−1.8	−15.5	0.5
P280	$[M+H]^+$	$C_{14}H_{21}N_2O_4$	281.1505	281.1496	0.9	3.2	5.5
	$[M+H\text{-}C(CH_3)_2]^+$	$C_{11}H_{15}N_2O_4$	239.1049	239.1026	2.3	9.6	5.5
	$[M+H\text{-}C(CH_3)_2\text{-}NH_3\text{-}CO]^+$	$C_{10}H_{12}NO_3$	194.0822	194.0812	1.0	5.1	5.5
	$[M+H\text{-}C(CH_3)_2\text{-}NH_3\text{-}CO\text{-}H_2O]^+$	$C_{10}H_{10}NO_2$	176.0713	176.0706	0.7	4.0	6.5
	$[M+H\text{-}C(CH_3)_2\text{-}NH_3\text{-}CO\text{-}H_2O\text{-}NH_3]^+$	$C_{10}H_7O_2$	159.0440	159.0441	−0.1	−0.6	7.5
	$[M+H\text{-}C(CH_3)_2\text{-}CH_2NH_2\ \text{-}H_2O\text{-}CH_2CONH_2]^+$	$C_8H_5O_2$	133.0282	133.0284	−0.2	−1.5	6.5
	$[M+H\text{-}C(CH_3)_2\text{-}NH_3\text{-}CO\text{-}H_2O\text{-}CH_2\text{-}NH_2\text{-}C_2H]^+$	$C_7H_5O_2$	121.0257	121.0284	−2.7	−22.3	5.5
	$[M+H\text{-}O\text{-}OC_6H_4CH_2CONH]^+$	$C_6H_{14}NO$	116.1066	116.1070	−0.4	−3.4	0.5
P282	$[M+H]^+$	$C_{14}H_{23}N_2O_4$	283.1656	283.1652	0.4	1.4	4.5
	$[M+H\text{-}NH_3]^+$	$C_{14}H_{20}NO_4$	266.1389	266.1387	0.2	0.7	5.5
	$[M+H\text{-}C(CH_3)_2]^+$	$C_{11}H_{17}N_2O_4$	241.1163	241.1183	−2.0	−8.3	4.5
	$[M+H\text{-}C(CH_3)_2\text{-}NH_3]^+$	$C_{11}H_{14}NO_4$	224.0935	224.0917	1.8	8.0	5.5
	$[M+H\text{-}C(CH_3)_2\text{-}NH_3\text{-}H_2O]^+$	$C_{11}H_{12}NO_3$	206.0820	206.0812	0.8	3.9	6.5
	$[M+H\text{-}C(CH_3)_2\text{-}NH_3\text{-}CO]^+$	$C_{10}H_{14}NO_3$	196.0972	196.0968	0.4	2.0	4.5
	$[M+H\text{-}C(CH_3)_2\text{-}NH_3\text{-}H_2O\text{-}CO]^+$	$C_{10}H_{12}NO_2$	178.0861	178.0863	−0.2	−1.1	5.5
	$[M+H\text{-}C(CH_3)_2\text{-}NH_3\text{-}CO\text{-}H_2O\text{-}NH_3]^+$	$C_{10}H_9O_2$	161.0595	161.0597	−0.2	−1.2	6.5
	$[M+H\text{-}C(CH_3)_2\text{-}NH_3\text{-}CO\text{-}H_2O\text{-}CHNH_2]^+$	$C_9H_9O_2$	149.0594	149.0597	−0.3	−2.0	5.5
	$[M+H\text{-}OH\text{-}OC_6H_4CH_2CONH_2]^+$	$C_6H_{14}NO$	116.1069	116.1070	−0.1	−0.9	0.5

[a] DBE, double bond equivalent.

matrix, were analyzed in a full-scan mode at QqToF–MS instrument. The full-scan experiments performed on the UPLC-QqToF instrument showed the appearance of 6 new peaks concurrent with the disappearance of ATL in the samples from both TiO_2 and photo-Fenton experiments (see Supporting Information, Figure S1). Table 2 summarizes the exact masses of molecular ions and fragment ions, together with recalculated mass errors and double bond equivalents (DBEs) given by the software. The data presented in Table 2 were obtained under optimized conditions of collision energy and cone voltage in ESI (+)-MS^2 experiments on the QqToF instrument, using an identification program of QqToF instrument with mass measurements accuracy threshold of 5 ppm. In the case of ATL, the most abundant signals detected were the m/z 190 fragment ion formed by the loss of 77 Da

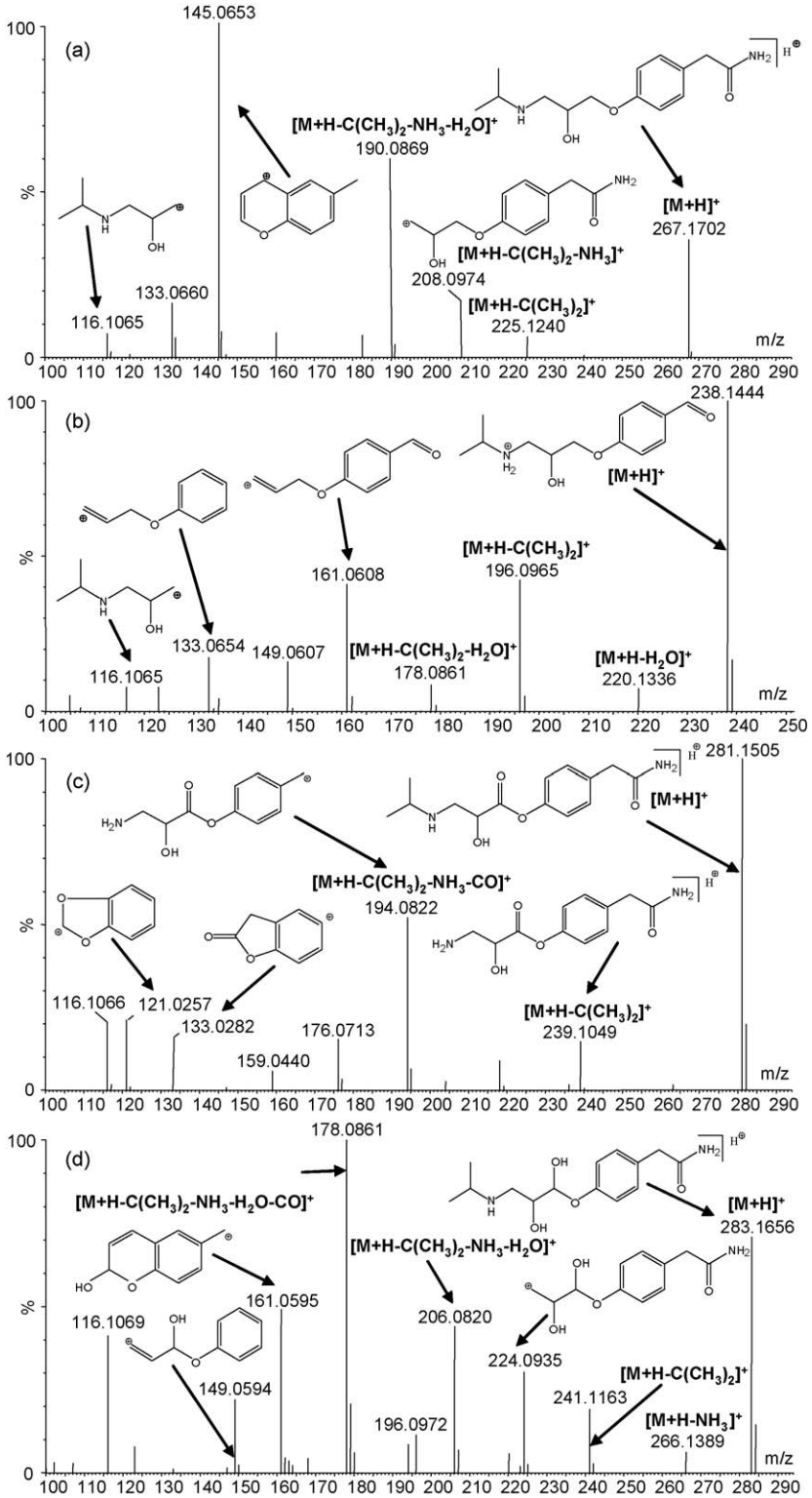

Fig. 5. Spectra obtained in ESI(+)-MS^2 experiments at QqToF instrument (cone voltages 25 V, collision energies 15–25 eV) for atenolol (ATL) and the intermediate products of its photocatalytic degradation: (a) ATL and (b) P237, (c) P281, and (d) P283.

(i.e., isopropylamine and water), and *m*/*z* 145 fragment ion, formed from *m*/*z* 190 after the cleavage of a CO molecule and intermolecular cyclization and rearrangement (see Fig. 5a).

The signal appearing at a retention time (t_R) of 4.5 min was identified as $[M+H]^+$ 238 molecular ion and labeled as intermediate product P237. The difference in mass of 29 Da in comparison with the molecular ion of ATL was assumed to be due to the loss of amide group from the molecule, and addition of oxygen to alkyl group attached to the ring after hydrogen abstraction by •OH radical attack, resulting in keto derivative.

The neutral loss of water from the protonated molecule of P237 afforded the *m*/*z* 220 fragment ion (see Fig. 5b). On the other side, the cleavage of isopropyl group from $[M+H]^+$ 238 resulted in the formation of very abundant *m*/*z* 196 fragment ion, which by further loss of water gave the *m*/*z* 178 fragment ion. Possibly the cleavage of methylamine moiety from *m*/*z* 178 afforded the fragment ion *m*/*z* 161. The loss of methyl amino isopropyl group and hydroxyl group probably led to the formation of the *m*/*z* 149 fragment ion. Similar to the spectrum of ATL the fragment ion *m*/*z* 133 was also observed in the fragmentation pattern of P237, formed by the loss of amino isopropyl moiety, water, and aldehyde and acetamide group for P237 and atenolol, respectively. Another fragment that was mutual for both $[M+H]^+$ 267 and $[M+H]^+$ 238 was the *m*/*z* 116 fragment ion, obtained by the scission of C–O bond and loss of *p*-hydroxyphenyl acetamide. The rupture of C–O bond in the $[M+H]^+$ 238 and intramolecular cyclization and rearrangement could be responsible for the presence of the *m*/*z* 123 fragment ion.

Two more intermediates arose at t_R = 2.9 and 3.45 min that corresponded to P282 and P280 products with molecular ions $[M+H]^+$ 283 and 281, respectively. The exact positions of the •OH radical attacks could be deduced from analysis of the MS^2 spectra performed on a QqToF instrument and measured accurate masses of precursor and fragment ions, illustrated in Fig. 5c and d.

In comparison with the spectrum of ATL, both P280 and P282 oxidation products show the characteristic loss of isopropyl group (42 Da) that afforded fragment ions *m*/*z* 239 and 241, respectively. Following loss of acetamide group from *m*/*z* 239 and 241 generated fragment ions *m*/*z* 194 and 196 that with further cleavage of water gave *m*/*z* 176 and 178 fragment ions, respectively. After further loss of ammonia from *m*/*z* 176 and 178 and intramolecular cyclization fragment ions *m*/*z* 159 and 161 were formed, respectively. In the fragmentation pattern of P280 two more fragment ions were detected at *m*/*z* 133.028 and 121. The *m*/*z* 133.028 was possibly formed from the $[M+H]^+$ 281 molecular ion by the loss of methyl isopropylamine group, water and acetamide moiety, and intramolecular cyclization afterwards. The *m*/*z* 121 fragment ion could be reasoned out by the cleavage of amino group and terminal acetylene group, and methyl group at the aromatic ring in the *m*/*z* 176 fragment ion. For both P280 and P282 characteristic fragment ion at *m*/*z* 116 was observed, thus confirming again the presence of the isopropyl portion of the molecule.

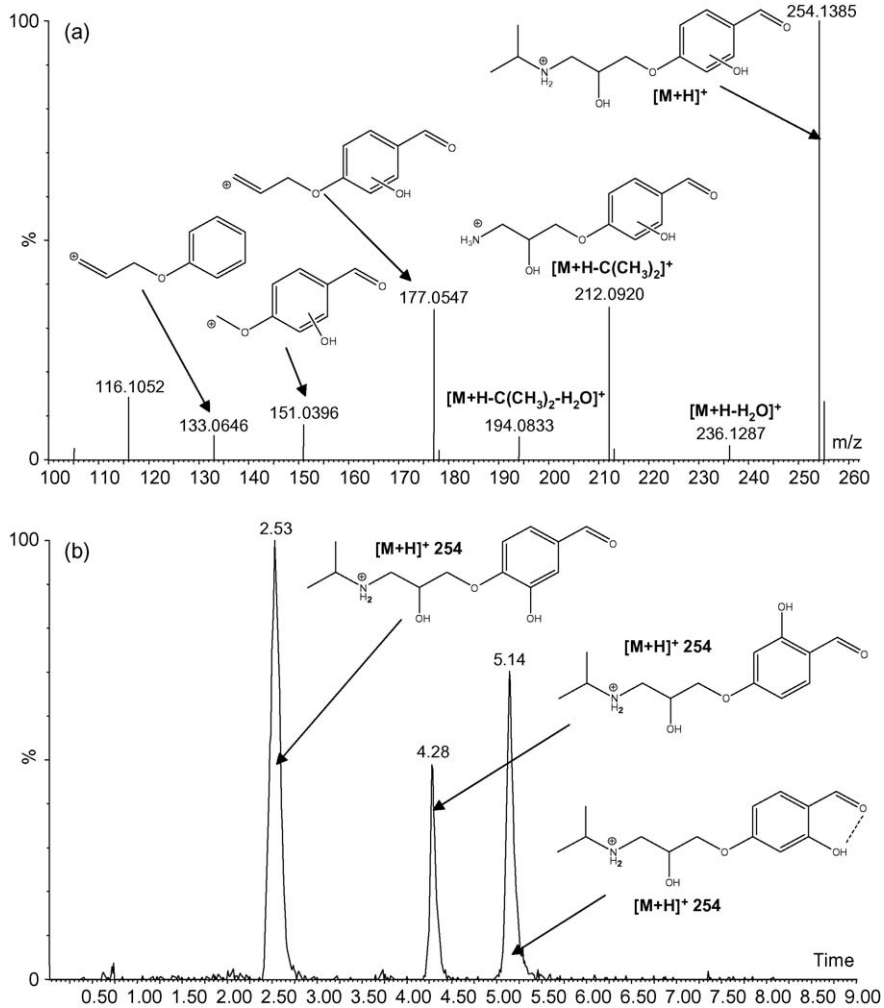

Fig. 6. (a) Spectra obtained in ESI(+)-MS^2 experiments at QqToF instrument for intermediate product P253 (cone voltages 25 V, collision energies 20 eV), (b) extracted ion chromatogram (XIC) of $[M+H]^+$ 254 molecular ion from a sample taken during photo-Fenton experiment.

On the other side, in the spectrum of P282 a low intensity signal was recorded at *m*/*z* 266, corresponding to the loss of ammonia from acetamide moiety of the $[M+H]^+$ 283 molecular ion. Similar to the spectrum of ATL ($[M+H]^+$ 267 → *m*/*z* 208, *m*/*z* 190), two more ions were observed in the fragmentation pattern of P282 at *m*/*z* 224 and 208, representing the subsequent losses of isopropylamine and water, respectively. Moreover, the fragment ion *m*/*z* 149 was detected, possibly formed by the loss of isopropylamine, water and acetamide group from the $[M+H]^+$ 283 molecular ion.

At t_R = 2.5, 4.3 and 5.15 min three peaks with the same molecular ion $[M+H]^+$ 254 were detected. Since they presented the same losses in the mass spectra with the same relative ion signal intensities they were all labelled as P253, whereas the non-specific •OH radical attack at P237 intermediate was assumed to be responsible for their formation (see Fig. 6a). Although the obtained analytical information does not allow the prediction of the precise position of the attack, based on the fact that the all three peaks exhibited the same fragmentation pattern it was assumed that the hydroxylation took place at the activated aromatic ring. Since there were only two available positions for the addition of the •OH radical, *ortho*- and *meta*- to the aldehyde group, three different peaks could be explained by the intramolecular hydrogen bond between the hydrogen of the –OH group attached to the ring and oxygen of the aldehyde group (*ortho*-isomer) or the absence of one (*meta*-isomer). It could be assumed that in the case of *meta*-isomer the hydrogen bond with the ether oxygen from the alkyl backbone would be less probable since the electron density at ether oxygen is lowered by the alkyl substituent. The presence of intramolecular hydrogen bond has been previously reported for *ortho*-isomers of hydroxylated photocatalytic intermediates of bezafibrate [24], whereas an increase in t_R was observed due to the decrease in polarity of the molecule. Thus, the most polar compound appearing at t_R = 2.5 min is probably the *meta*-hydroxylated intermediate P253, whereas the compounds appearing at t_R = 4.3 and 5.15 min could be the two *ortho*-derivatives, without and with the intramolecular hydrogen bond, respectively (see Fig. 6b).

The loss of water from $[M+H]^+$ 254 generated low intensity *m*/*z* 236 fragment ion. The loss of isopropyl moiety brought forth the *m*/*z* 212 fragment, which was further dehydrated to the *m*/*z* 194 fragment ion. Analogous to the formation of the *m*/*z* 161 fragment ion in the spectrum of P237, *m*/*z* 177 fragment ion was observed in the spectrum of P253 (i.e., loss of methylamine group from the *m*/*z* 194). The following neutral loss of C_2H_2 from the *m*/*z* 177 resulted in the low intensity *m*/*z* 151 fragment ion. Moreover, the characteristic fragment ions *m*/*z* 116 and 133 detected in the spectrum of ATLl and P237 were also seen in the fragmentation pattern of P253.

3.6. Mechanism of photocatalytic degradation of ATL

Considering the identified intermediate products of photo-Fenton and photocatalytic degradation of ATL, they can be lined together through the photodegradation pathway presented in Scheme 2. The intermediate product P237 was formed by the loss of amide group, abstraction of hydrogen by the •OH radical attack on the alkyl group attached to the ring and addition of oxygen. The + 2 oxidation state of C atom in the amide group should favor the •OH radical attack at this atom, generating $CONH_2$• radical followed by formation of carbamic acid [33]. Carbamic acid eventually goes through photo-assisted hydrolysis and nitrogen is released as NH_4^+ ion [36]. Then, the •OH radical attack at C atom next to the ether oxygen afforded the 283 products, whereas either further oxidation of the newly added –OH group or the addition of O_2 after hydrogen abstraction gave the keto-tautomer 281. This reaction mechanism via keto-enol tautomers has been previously reported for the photo-Fenton degradation of diclofenac [23]. In the case of TiO_2 photocatalytic degradation, enol tautomer was more abundant than the keto derivative, whereas in the photo-Fenton experiments

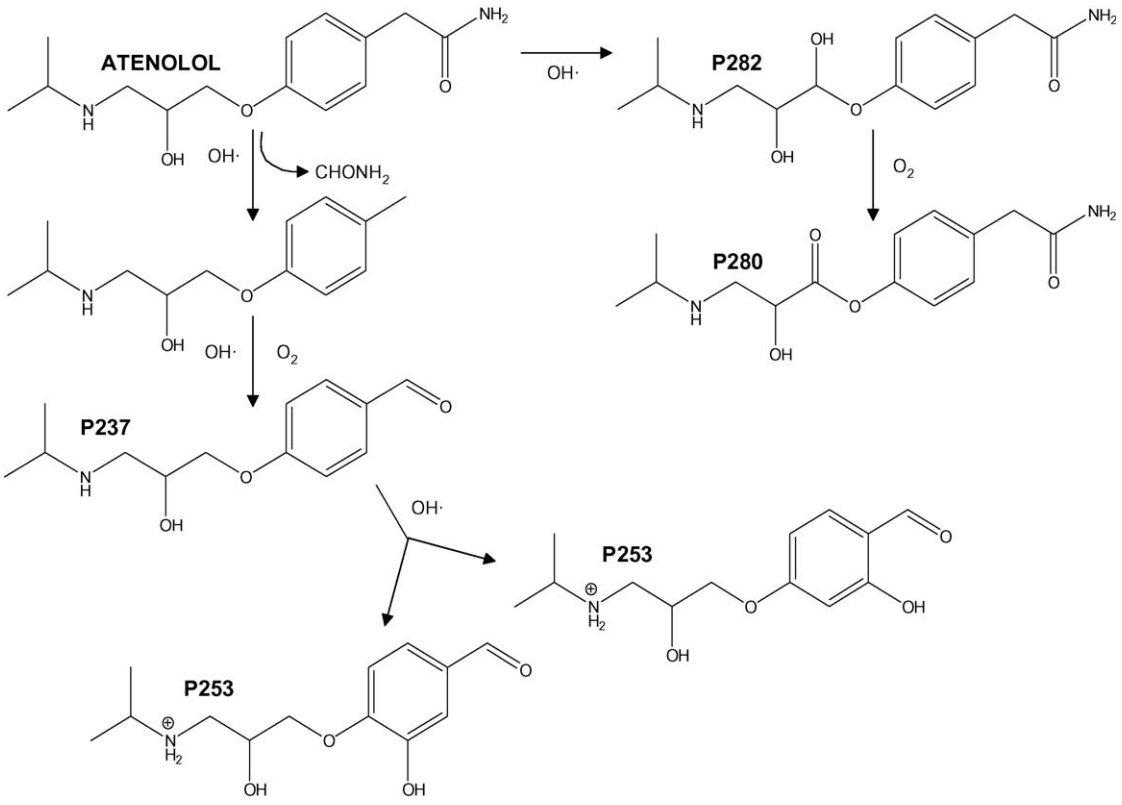

Scheme 2. Proposed photocatalytic degradation pathway of ATL in aqueous solution by solar TiO_2 and photo-Fenton treatment.

they seemed to be in equilibrium. Finally, three intermediate products P253 were formed as a consequence of the non-selectivity of •OH radical, by hydroxylation of the aromatic ring of the P237 product. The most intense peak among P253 intermediates was seen for the product hydroxilated in *meta*-position relative to the aldehyde group at the aromatic ring. This greater stability of *meta*-isomer could be expected since the R-oxy substituent has an activating effect on the aromatic ring increasing its electron density, whereas the amide group acts as a deactivating substituent due to the electron withdrawing effect [37,38].

Among the detected intermediates, P237, P253 and P283 are reported for the first time, whereas a transformation product with molecular ion $[M+H]^+$ 281 was previously detected on a LTQ Orbitrap mass spectrometer in a study by Medana et al. [27], although the exact position of •OH radical attacks was not identified. All the intermediates were rapidly degraded, whereas their evolution profiles together with the disappearance of ATL are presented in Figure S2 of Supporting Information. The profiles were only qualitative, since for the newly identified transformation products there were no analytical standards available to ensure their quantitative analysis. The formation of all 6 intermediates went simultaneously with the decrease in ATL concentration, whereas all transformation products were degraded after the first 1.5 and 2.5 h in TiO_2-assisted photodegradation and after 1 and 1.5 h in the photo-Fenton experiments with distilled and synthetic wastewater, respectively. As far as TOC is concerned, its decomposition was rather slow and incomplete during TiO_2 assisted photocatalysis, with around 40% and 13% of mineralization achieved with distilled water and SE, respectively. The degradation of DOC in the photo-Fenton experiment with distilled water was more efficient (i.e., 74% after 35.5 min of irradiation), whereas in the SE only 13% of the initial organic matter was mineralized when ATL was completely eliminated.

4. Conclusions

Degradation of ATL and ACTP dissolved in SE in TiO_2 and photo-Fenton solar photocatalysis was complete and followed pseudo-first order reaction kinetics. The photo-Fenton treatment proves to be more efficient for degradation of ATL and ACTP than the TiO_2 photocatalytic treatment. Lower reaction rate for S.E. compared with distilled water were observed in all cases, mainly due to the detrimental effect of other organic compounds typically present in municipal wastewater effluents. It demonstrated the necessity of evaluating kinetics taking into account the influence of the matrix when applying AOPs for the treatment of wastewater.

QqToF coupled to a UPLC has found to be a powerful tool for elucidating the exact structure of intermediate products formed during TiO_2 photocatalyzed and photo-Fenton reactions of ATL. The pathways of their photocatalytic degradation in both TiO_2 and photo-Fenton processes start with hydroxylation (i.e., •OH radical attack), dealklylation, deamination, oxidation by •OH radicals and O_2 and reduction by conductive band electrons. Moreover, investigations with SE indicated that the photodegradation followed the same transformation routes as in the distilled water.

The intermediate products identified are formed in the initial steps of degradation of ATL, whereas the analysis of samples taken after long reaction times showed a complete disappearance of all intermediate products and also primary compounds. It can be assumed that after formation of aromatic derivatives, cleavage of benzene ring will take place for ATL, while different aliphatic products (as carboxylic acids) are subsequently formed before complete mineralization. Carboxylic acids were detected at the end of TiO_2 and photo-Fenton experiments, demonstrating that the parent compounds and the main intermediates products are finally degraded to organic short-chain acids before being mineralized. Therefore, treatment time should be enough to produce such compounds, but complete mineralisation is not necessary.

Acknowledgments

The study was financially supported by the EU project INNOVA MED (INCO-CT- 2006-517728) and the MICINN (Spain) "Programa de Acceso y Mejora de Grandes Instalaciones Científicas Españolas" (Plataforma Solar de Almería, GIC-05-17). Jelena Radjenovic gratefully acknowledges the JAE Program (Junta para la Ampliación de los Estudios), co-financed by CSIC (Consejo Superior de Investigaciones Científicas) and European Social Funds. Carla Sirtori wish to thank the CAPES foundation-Ministry of Education of Brazil for the Ph.D. Research grant (BEX Processo: 3763-05-6).

Appendix A. Supplementary data

Supplementary data associated with this article can be found, in the online version, at doi:10.1016/j.apcatb.2009.02.013.

References

[1] D.W. Kolpin, E.T. Furlong, M.T. Meyer, E.M. Thurman, S.D. Zaugg, L.B. Barber, H.T. Buxton, Environ. Sci. Technol. 36 (2002) 1202.
[2] B. Halling-Sørensen, S. Nors Nielsen, P.F. Lanzky, F. Ingerslev, H.C. Holten Lützhøft, S.E. Jørgensen, Chemosphere 36 (1998) 357.
[3] E.M. Golet, A. Strehler, A.C. Alder, W. Giger, Anal. Chem. 74 (2002) 5455.
[4] M.I. Aguilar, S.J. Hart, I.C. Calder, J. Chromatogr. 426 (1988) 315.
[5] C. Dollery, Therapeutic Drugs, Edinburgh, London, 1991.
[6] B.I. Escher, N. Bramaz, M. Richter, J. Lienert, Environ. Sci. Technol. 40 (2006) 7402.
[7] J. Radjenovic, M. Petrovic, D. Barcelo, Trends Anal. Chem. 26 (2007) 1132.
[8] M. Maurer, B.I. Escher, P. Richle, C. Schaffner, A.C. Alder, Water Res. 41 (2007) 1614.
[9] Q.T. Liu, H.E. Williams, Environ. Sci. Technol. 41 (2007) 803.
[10] V. Andrisano, R. Gotti, A. Leoni, V. Cavrini, J. Pharm. Biomed. Anal. 21 (1999) 851.
[11] Y. Liu, X. Yang, Y. Gao, Huanjing Kexue/Chin. J. Environ. Sci. 28 (2007) 1274.
[12] S. Malato, J. Blanco, D.C. Alarcón, M.I. Maldonado, P. Fernández-Ibáñez, W. Gernjak, Catal. Today 122 (2007) 137.
[13] O. González, C. Sans, S. Esplugas, J. Hazard. Mater. 146 (2007) 459.
[14] L.A. Perez Estrada, S. Malato, A. Agüera, A.R. Fernández-Alba, Catal. Today 129 (2007) 207.
[15] O.K. Dalrymple, D.H. Yeh, M.A. Trotz, J. Chem. Technol. Biotechnol. 82 (2007) 121.
[16] J.M. Herrmann, Top. Catal. 34 (2005) 49.
[17] A. Fujishima, T.N. Rao, D.A. Tryk, J. Photochem. Photobiol. C: Photochem. Rev. 1 (2000) 1.
[18] M.R. Hoffmann, S.T. Martin, W. Choi, D.W. Bahnemann, Chem. Rev. 95 (1995) 69.
[19] J.J. Pignatello, Environ. Sci. Technol. 26 (1992) 944.
[20] S.Y. Panshin, D.S. Carter, E.R. Bayless, Environ. Sci. Technol. 34 (2000) 2131.
[21] P. Calza, M. Pazzi, C. Medana, C. Baiocchi, E. Pelizzetti, J. Pharm. Biomed. Anal. 35 (2004) 9.
[22] T.E. Doll, F.H. Frimmel, Water Res. 38 (2004) 955.
[23] L.A. Pérez-Estrada, S. Malato, W. Gernjak, A. Agüera, E.M. Thurman, I. Ferrer, A.R. Fernández-Alba, Environ. Sci. Technol. 39 (2005) 8300.
[24] D.A. Lambropoulou, M.D. Hernando, I.K. Konstantinou, E.M. Thurman, I. Ferrer, T.A. Albanis, A.R. Fernández-Alba, J. Chromatogr. A 1183 (2008) 38.
[25] S. Zbaida, R. Kariv, P. Fischer, J. Silman-Greenspan, Z. Tashma, Eur. J. Biochem. 154 (1986) 603.
[26] X. Zhang, F. Wu, X. Wei Wu, P. Chen, N. Deng, J. Hazard. Mater. 157 (2008) 300.
[27] C. Medana, P. Calza, F. Carbone, E. Pelizzeti, H. Hidaka, C. Baiocchi, Rapid Commun. Mass Spectrom. 22 (2008) 301.
[28] OECD Guidelines for Testing of Chemicals, Simulation Test-Aerobic Sewage Treatment 303A, 1999.
[29] S. Malato, J. Blanco, C. Richter, M. Vincent, Solar Energy 56 (1996) 401.
[30] R.F.P. Nogueira, M.C. Oliveira, W.C. Paterlini, Talanta 66 (2005) 86.
[31] I. Ferrer, E.M. Thurman, Rapid Commun. Mass Spectrom. 21 (2007) 2538.
[32] A.G. Trovó, S.A.S. Melo, R.F.P. Nogueira, J. Photochem. Photobiol. A: Chem. 198 (2008) 215.
[33] P. Calza, E. Pelizzetti, C. Minero, J. Appl. Electrochem. 35 (2005) 665.
[34] V. Kavitha, K. Palanivelu, Chemosphere 55 (2004) 1235.
[35] L.A. Pérez Estrada, S. Malato, A. Aguera, A.R. Fernández-Alba, Catal. Today 129 (2007) 207.
[36] C. Maillard-Dupuy, C. Guillard, H. Courbon, P. Pichat, Environ. Sci. Technol. 28 (1994) 2176.
[37] M.M. Huber, S. Canonica, G.-Y. Park, U. Von Gunten, Enivron. Sci. Technol. 37 (2003) 1016.
[38] J. Hoigné, H. Bader, Water Res. 17 (1983) 185.